Inorganic Chemistry

Article

pubs.acs.org/IC

The Propensity of Uranium-Peroxide Systems to Preserve Nanosized Assemblies

Mateusz Dembowski,[†] Christopher A. Colla,[‡] Ping Yu,[§] Jie Qiu,[∥] Jennifer E. S. Szymanowski,[∥] William H. Casey,[‡,⊥] and Peter C. Burns*[,†,∥]

[†]Department of Chemistry and Biochemistry, University of Notre Dame, Notre Dame, Indiana 46556, United States

[‡]Department of Earth and Planetary Sciences, University of California, Davis, California 95616, United States

[§]The Keck NMR Facility, University of California, Davis, California 95616, United States

[∥]Department of Civil and Environmental Engineering and Earth Sciences, University of Notre Dame, Notre Dame, Indiana 46556, United States

[⊥]Department of Chemistry, University of California, Davis, California 95616, United States

Supporting Information

ABSTRACT: Understanding the stability fields and decomposition products of various metal- and actinide-oxide nanoclusters is essential for their development into useful materials for industrial processes. Herein, we explore the spontaneous transformation of the sulfate-centered, phosphate functionalized uranyl peroxide nanocluster $\{U_{20}P_6\}$ to $\{U_{24}\}$ under aqueous ambient conditions using time-resolved small-angle X-ray scattering, Raman, and ^{31}P NMR spectroscopy. We show that the unusual μ-η^1:η^2 bridging mode of peroxide between uranyl ions observed in $\{U_{20}P_6\}$ may lead to its rapid breakdown in solution as evidenced by liberation of phosphate groups that were originally present as an integral part of its cage structure. Remarkably, the uranyl peroxide moieties present after degradation of $\{U_{20}P_6\}$ undergo cation-mediated reassembly into the $\{U_{24}\}$ cluster, demonstrating the propensity of the uranyl peroxide systems to preserve well-defined macro-anions.

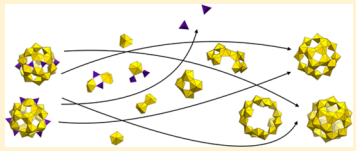

INTRODUCTION

Polyoxometalates (POMs) are a diverse group of well-defined metal oxide ions classically constructed of Group V and Group VI transition metals in their highest oxidation states.[1] Since their initial discovery in 1826[2] and first structural characterization in 1933,[3,4] many studies reflect their versatile nature and applicability in areas ranging from catalysis to medicine.[5−10] Notably, POMs represent an excellent model for detailed studies of metal oxide solid-state materials and their interactions with environmental contaminants.[11−14] The recently emerged group of actinyl peroxide nanoclusters, in addition to extending the scope of POM chemistry to early 5f block elements, challenges our understanding of the fundamental behavior of actinide elements in solution.[15−18]

From a structural standpoint, actinyl (uranyl) peroxide nanoclusters are similar to *Keplerates* in that they are composed of condensed uranyl-oxide polyhedra forming hollow, anionic clusters.[18,19] One key difference is the presence of the actinyl ion (UO_2^{2+}) containing two relatively chemically inert *−yl* oxygens in a *trans* arrangement, as compared to the *cis* conformation commonly observed in transition metals, that in conjunction with peroxide ligands favor capsule architectures.[20] Uranyl peroxide cages and *Keplerates* are typically characterized by high molecular symmetry, although a few members of the former group depart from this trend.[17,21,22] Further similarities include the ability to amend the size and charge of these clusters[23−25] and the presence of molecular pores that allow cation exchange between the cavity and the surrounding solution or interstitial space in a crystal.[26−29] Uranyl peroxide nanoclusters attracted considerable attention due to their potential importance in the environmental mobility of actinides, and applications in advanced nuclear fuel cycles.[30−33] To date, publication of more than 60 unique uranyl peroxide structures showcases their significant structural and chemical diversity.[17]

Considering the attention POMs have received in the past, including but not limited to the extensive potentiometric studies conducted on labile cluster-containing solutions,[34−37] it is surprising to find relatively few studies of the stability fields, and dissociation products, of the relatively inert clusters.[38−42] Such studies are essential if these POMs are to be useful in industrial-scale applications. Applications require a confident understanding of the reactions that these POMs undergo under various conditions, including the identity of their dissociation products. The importance of such studies becomes evident when considering the example of the ε-Al_{13} Keggin polycation, which has been demonstrated to undergo, under ambient conditions, a spontaneous, monomer mediated condensation reaction to form the Al_{30} cluster.[43,44]

Herein, we report the spontaneous dissociation of the $\{U_{20}P_6\}$ cluster containing peroxide ligands in an unusual μ-η^1:η^2 bridging mode[45] under ambient aqueous conditions. Multinuclear magic-angle spinning (MAS) NMR experiments afforded unambiguous evidence of cluster stability prior to

Received: May 1, 2017
Published: August 7, 2017

DOI: 10.1021/acs.inorgchem.7b01095
Inorg. Chem. 2017, 56, 9602−9608

dissolution, while time-resolved small-angle X-ray scattering (SAXS), ^{31}P NMR, and Raman spectroscopy demonstrated its rapid dissociation in water. Single crystal X-ray diffraction of crystalline material obtained by slow evaporation of solutions containing dissolved $\{U_{20}P_6\}$ confirmed the identity of the restructured uranyl peroxide species as $\{U_{24}\}$.

EXPERIMENTAL SECTION

Warning! *Uranium-238 is a weak alpha emitter (α = 2.467 MeV) and should be handled by trained personnel in laboratories equipped and licensed for work with radioactive elements.*

General Considerations. Uranyl nitrate hexahydrate $(UO_2(NO_3)_2{\cdot}6H_2O$, International Bio-Analytical Industries, Inc.), hydrogen peroxide (H_2O_2, 30% aqueous solution, EMD Millipore), lithium hydroxide monohydrate ($LiOH{\cdot}H_2O$, EMD Millipore), sodium sulfite (Na_2SO_3, Sigma-Aldrich), phosphoric acid (H_3PO_4, 85%, Sigma-Aldrich), and deuterium oxide (98% D_2O, Cambridge Isotope Laboratories, Inc.) were purchased from commercial suppliers and used without further purification.

Phosphate functionalized uranyl peroxide nanoclusters are abbreviated as $\{U_nP_m\}$, where n corresponds to the number of uranyl peroxide polyhedra and m is the number of phosphate (PO_4^{3-}) bridges. Nonfunctionalized uranyl peroxide nanoclusters are designated as $\{U_n\}$, where n is the number of uranyl peroxide polyhedra. The $\{U_{20}P_6\}$ cluster was synthesized according to published procedures.[45] The identity and purity of the obtained species was confirmed by single crystal X-ray diffraction and solid-state Raman spectroscopy (see the Supporting Information). Diffusion-ordered spectroscopy measurements were conducted on solutions prepared by placing 5 mg of crystalline $\{U_{20}P_6\}$ in 1 mL of deuterated water. Time-resolved measurements were conducted on solutions prepared by placing 20 mg of crystalline $\{U_{20}P_6\}$ in 1 mL of ultrapure (SAXS and Raman) or deuterated water (NMR) and 100 μL of 0.1 M $LiNO_3$. The mixtures were subsequently vortexed and centrifuged to remove any residual solid particles, resulting in clear, bright yellow (D_2O, DOSY NMR) or golden-orange solutions (D_2O + $LiNO_3$, time-resolved NMR, SAXS, and Raman). Changes in pH conditions of solutions prepared by using ultrapure water (see above) were monitored as a function of time and are available in the Supporting Information.

Single Crystal X-ray Diffraction. Crystals suitable for X-ray diffraction were transferred, with a small amount of mother liquor, into oil, visually inspected, and mounted on cryoloops. A full sphere of data was collected for each crystal centered under a stream of nitrogen gas (100 K) using a Bruker APEX II Quazar diffractometer equipped with a microsource sealed tube (multilayer monochromated Mo$K\alpha$ X-rays). Frame widths of 0.5° in ω and an exposure time of 10 s were implemented in all data collections. Data integrations including corrections for Lorentz, polarization, and background effects were performed using the Bruker APEX III software with corrections applied using SADABS.[46] SHELXTL[47,48] was used for structure solution and refinement. Note: This manuscript does not report crystal structure determinations, but does include determination of unit cell dimensions to confirm the identity of observed crystalline phases. Basic unit cell parameters for the $\{U_{20}P_6\}$ and $\{U_{24}\}$ clusters are available in the Supporting Information.

NMR Spectroscopy. Time-resolved ^{31}P NMR spectra were recorded using a 500 MHz Varian INOVA spectrometer (11.57 T) with 14.8 ms pulse length, 56 dB power level attenuation, 5 s relaxation delay, and 64 scans using an automated collection sequence resulting in a 15 min delay between each consecutive collection.

Diffusion-ordered spectroscopy (DOSY) data were recorded using a 500 MHz Bruker DRX NMR spectrometer (11.74 T). A 5 mm Bruker PABBO Broad-band /^{19}F – ^{1}H/^{2}H probe equipped with Z-gradients was used for data acquisition. Data were acquired using the stimulated-echo *stegp1s* 2D pulse sequence. The diffusion gradient length (δ) and diffusion delay time (Δ) were set to 2000 μs and 0.5 s, respectively. The gradient strength was set to 100% (10 A or 53 G/cm^{-1}), and the total number of slices acquired was 16, with 64 scans per slice. A linear ramp was used in the collection of the diffusion data.

Solid-state magic-angle spinning (MAS) NMR spectra were recorded on a Bruker AVANCE 500 MHz NMR spectrometer (11.74 T) equipped with a Bruker double resonance 2.5 mm MAS probe. Crystalline $\{U_{20}P_6\}$ was ground to a powder and subsequently loaded into 2.5 mm zirconia rotors with Vespel caps. Samples were spun at 20 kHz. ^{1}H chemical shifts were externally referenced to a secondary external standard adamantine with respect to tetramethylsilane (δ = 0 ppm). ^{7}Li, ^{23}Na, and ^{31}P chemical shifts were externally referenced to 1 M LiCl, 1 M NaCl, and 85% H_3PO_4, respectively. Details about pulse sequences used in each collection are available in the Supporting Information.

Small-Angle X-ray Scattering (SAXS). SAXS measurements were conducted on a Bruker Nanostar equipped with a Cu microfocus source, Montel multiplayer optics, and a HiSTAR multiwire detector. Each sample was introduced into the collection chamber through a flow cell located 26.3 cm from the detector. Data were collected for 1 h, including a sample of pure water for the purpose of accounting for background effects.

Raman Spectroscopy. Raman spectra were collected on a Bruker Sentinel system equipped with a fiber optic probe, 785 nm excitation source, and thermoelectrically cooled CCD detector. Solid and solution sample spectra were acquired in the range from 80 to 3200 cm^{-1} using three 15 s exposures at 148 and 400 mW laser power settings, respectively.

RESULTS

The phosphate functionalized $\{U_{20}P_6\}$ cluster represents a unique subclass of polyoxometalate ions because it incorporates the peroxide ligand in a highly unusual μ-η^1:η^2 bridging mode. The presence of multiple NMR-active nuclei in $\{U_{20}P_6\}$ (^{31}P, ^{23}Na, ^{7}Li, and ^{1}H) makes it an excellent candidate for solid-state and solution studies, especially in the light of its highly distorted dodecahedral geometry (Figure 1). Prior magic-angle

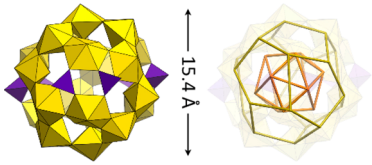

Figure 1. (left) Polyhedral and (right) graphical representation of the $\{U_{20}P_6\}$ cluster. Yellow and purple polyhedra represent uranium and phosphate, respectively. On the right, the yellow and orange lines represent the topological arrangements of the U and Na atoms, respectively.

spinning (MAS) NMR studies of nonfunctionalized uranyl peroxide clusters illustrated the particular usefulness of this technique by revealing an unexpected dynamic nature of encapsulated species, while also providing essential reference data used here.[49−51]

One-dimensional (1D) ^{1}H MAS NMR spectra of $\{U_{20}P_6\}$ reveal a single signal at 5.28 ppm assignable to the lattice water (Figure S2).[50] The absence of other signals in the ^{1}H spectrum reflects the lack of hydroxide bridges (μ-OH) or encapsulated waters in $\{U_{20}P_6\}$, in agreement with the crystallographically determined structure. ^{7}Li MAS NMR spectra show a single signal at 0.88 ppm assigned to lattice Li (Figure S3).[49] ^{23}Na MAS NMR spectra reveal two sites at −5.85 and −21.57 ppm (Figure S4), assigned to lattice and encapsulated Na atoms, respectively. This assignment is based on prior reports,[50] as well as the nutation experiments conducted in this study. The signal at −5.85 ppm exhibits a 90° pulse length of ca. 2.2 μs that is similar to that of ions in NaCl solutions, indicating its dynamic nature. On the other hand, the signal at −21.57 ppm is

DOI: 10.1021/acs.inorgchem.7b01095
Inorg. Chem. 2017, 56, 9602−9608

characterized by a shorter 90° pulse of ca. 1.6 μs, reflecting its more "rigid" structural environment. The information obtained from nutation experiments is in excellent agreement with the structurally determined positions of Na cations that are divided between the cavity of the cluster containing 12 Na ions arranged on the vertices of a regular icosahedron and 12 loosely bound Na ions located in the interstitial space. ^{31}P MAS NMR experiments reveal an asymmetric signal at 15.23 ppm (Figure S5) that is assigned to the phosphate bridges present within the cage of $\{U_{20}P_6\}$. Although its structure contains only one type of phosphate bridge, a detailed inspection of their environments reveal inequivalent distributions of cations in their vicinity. This inequivalency, when considered along with the mobile nature of Li and Na ions present in the interstitial space, probably accounts for the asymmetry of the observed NMR signal. Largely, the MAS NMR experiments conducted herein, as well as the time-resolved Raman spectroscopy studies of the crystalline material conducted in the original study,[45] provide compelling evidence that the $\{U_{20}P_6\}$ cluster is stable prior to dissolution.

Following the solid-state characterization of $\{U_{20}P_6\}$ using MAS NMR spectroscopy, diffusion-ordered spectroscopy (DOSY) measurements were conducted for dissolved species. DOSY exploits size-dependent diffusion rates of molecules as they undergo Brownian motion. The measured diffusion coefficients can be interpreted using the Stokes−Einstein equation to relate the NMR signals to molecule size. This approach permits the simultaneous detection of species spanning a range of sizes, as shown for metal- and actinide-oxide clusters.[52−56] NMR spectra of solutions of $\{U_{20}P_6\}$ in water (see the Experimental Section) exhibited a signal at 3.31 ppm that has a corresponding diffusion coefficient (D) and hydrodynamic radius (R_h) of 6.73 ± 0.12 m·s^{-2} and 3.10 ± 0.06 Å, respectively (Figure 2). The ^{31}P NMR signal arises from an

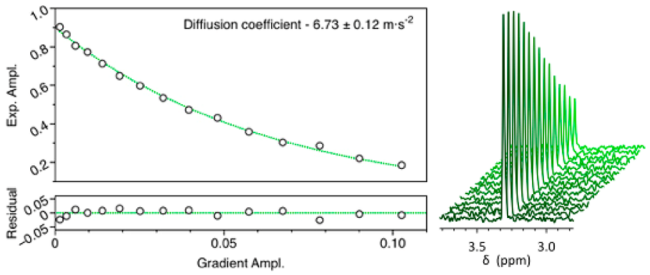

Figure 2. ^{31}P diffusion ordered spectroscopy (DOSY) NMR of solutions containing dissolved $\{U_{20}P_6\}$ cluster.

aqueous species that is significantly smaller than $\{U_{20}P_6\}$, for which the expected R_h value should exceed its crystallographically determined radius of 7.70 Å (Figure 1), due to the presence of a solvation shell. Comparison of the experimentally determined R_h with previously reported values for similar systems suggests that the signal at 3.31 ppm corresponds to species smaller than pyrophosphate ($P_2O_7^{4-}$, R_h = 4.02 ± 0.05 Å).[57] Given the composition of $\{U_{20}P_6\}$, the 3.31 ppm signal is assigned to free phosphate ions arising from dissociation of $\{U_{20}P_6\}$. This result is unexpected as the original report describing the synthesis and characterization of $\{U_{20}P_6\}$ included time-resolved SAXS measurements indicating its retention subsequent to dissolution in water, although it is noted that SAXS would not have been sensitive to the presence of free phosphate ions.[45]

During the DOSY experiments, we noted the relatively low solubility of $\{U_{20}P_6\}$ in water (<5 mg/mL) resulting in bright yellow solutions. Introduction of 100 μL of 0.1 M $LiNO_3$ per 1 mL of water resulted in increased solubility of crystalline $\{U_{20}P_6\}$ (ca. 10 mg/mL), producing golden yellow solutions, which over time reverted to the originally noted bright yellow color. Time-resolved ^{31}P NMR spectra of the solution obtained by dissolving the $\{U_{20}P_6\}$ cluster in Li-bearing water (Figure 3a) exhibited a new signal at 12.95 ppm, which decays over a

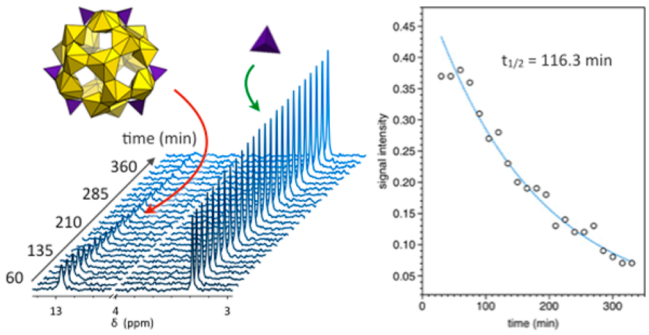

Figure 3. (left) Time-resolved ^{31}P NMR of Li bearing solution of $\{U_{20}P_6\}$. (right) Graph of the exponentially decaying signal at 12.95 ppm corresponding to the intact $\{U_{20}P_6\}$.

period of 400 min, with a corresponding increase of the free phosphorus signal at 3.31 ppm (see above). The decay of the 12.95 ppm signal coincides with the color changes, suggesting, along with the MAS NMR studies, that the golden yellow solution obtained by addition of $LiNO_3$ during the dissolution process likely corresponds to a mixture of the $\{U_{20}P_6\}$ cluster and products of its dissociation. Consequently, we assign the signal at 12.95 ppm to the intact $\{U_{20}P_6\}$ cluster. Its rapid decay, as indicated by the decrease of the 12.95 ppm signal, precluded reliable determination of its size via diffusion-ordered spectroscopy. The half-life ($t_{1/2}$) of the $\{U_{20}P_6\}$ cluster, under the experimental conditions, was determined to be ca. 116.3 min (Figure 3, right). Time-resolved studies on the $\{U_{20}P_6\}$/H_2O solutions (in the absence of $LiNO_3$) were not possible due to the weak intensity of the cluster signal at 12.95 ppm.

Time-resolved SAXS and Raman spectroscopy measurements were conducted on the Li bearing solutions containing the rapidly decaying $\{U_{20}P_6\}$ (Figure 4) to address the disparity of our current results with an earlier study that concluded $\{U_{20}P_6\}$ is stable in water.[45] Guinier analysis of the low-q regions of the scattering curves provided radii of gyration (R_g) ranging from 7.07 ± 0.03 Å at 10 min, to 7.67 ± 0.03 Å at 48 h

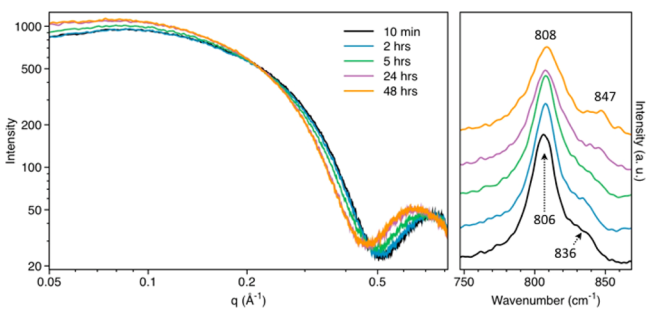

Figure 4. Time-resolved SAXS (left) and Raman spectroscopy (right) studies of Li bearing solutions of $\{U_{20}P_6\}$.

DOI: 10.1021/acs.inorgchem.7b01095
Inorg. Chem. 2017, 56, 9602−9608

(Table S2). The observed molecular size increases with time following the dissolution of $\{U_{20}P_6\}$, although it stabilizes by approximately 24 h. The distribution of SAXS-derived R_g values, DOSY spectra, and time-resolved ^{31}P NMR measurements all point to an in situ cluster-to-cluster interconversion that occurs upon dissolution of $\{U_{20}P_6\}$ in water, resulting in formation of a nonphosphate-functionalized cluster that is similar in size to $\{U_{20}P_6\}$. Solution-mode Raman spectroscopy (Figure 4) indicate the presence of uranyl peroxide nanoclusters with signals at 806 and 836 cm^{-1} (min 10) that evolve to 808 and 847 cm^{-1} (48 h). These are assigned to the symmetric stretch of the uranyl, $_{v1}(UO_2^{2+})$ and collective intramolecular vibration of the peroxide, $_{v}(O_2^{2-})$, respectively.[58,59] A recent study of uranyl peroxide nanoclusters notes similar Raman trends assigning peaks observed at 810 and 844 cm^{-1} (48 h) to formation of the $\{U_{24}\}$ cluster.[60]

Slow evaporation of solutions prepared by dissolving crystals of $\{U_{20}P_6\}$ in Li bearing water over a month afforded diffraction quality crystals characterized via single crystal X-ray diffraction as previously published Na $\{U_{24}\}$.[61] A secondary, bright yellow, microcrystalline phase coprecipitated with the crystals of $\{U_{24}\}$ and precluded a meaningful elemental analysis of the solid or useful MAS NMR studies (note: slow evaporation of solutions obtained by dissolving crystals of $\{U_{20}P_6\}$ in water, without addition of Li, yielded the same crystalline product). Figure 5

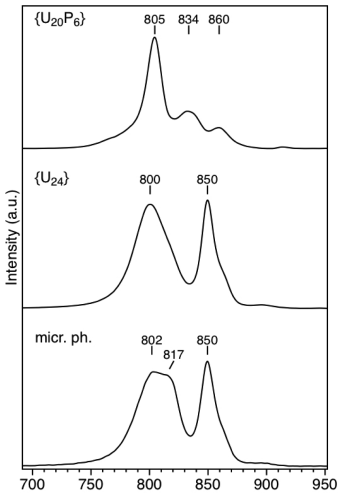

Figure 5. Comparison of solid-state Raman spectra of the $\{U_{20}P_6\}$ (top), $\{U_{24}\}$ (center), and microcrystalline phase (bottom).

compares the solid-state Raman spectra of $\{U_{20}P_6\}$ and $\{U_{24}\}$ crystals with the secondary microcrystalline phase. The spectra of Na $\{U_{24}\}$ crystals display characteristic uranyl and peroxide signals at 800 and 850 cm^{-1}, respectively. Despite a small red shift of the uranyl signal, which is sensitive to the identity of counter cations, these are in good agreement with those observed for this class of compounds.[59,60] Spectra of the secondary phase indicate it contains Na $\{U_{24}\}$ and a Li and/or Li/Na $\{U_{24}\}$ as evident from the 817 cm^{-1} signal. Our assignment is based on reported values for Li $\{U_{24}\}$ at 814 and 845 cm^{-1} as well as the Li-to-Na ratio noted in $\{U_{20}P_6\}$ of one to six, which necessitates formation of multiple salt variants due to limited availability of cations.[60]

DISCUSSION

The transformation of $\{U_{20}P_6\}$ in water to $\{U_{24}\}$ is spontaneous and relatively rapid at ambient conditions. However, this reaction involves a substantial topological change and rearrangement of uranyl polyhedra. The X-ray structure of $\{U_{20}P_6\}$ shows that its topology corresponds to a distorted dodecahedron (idealized D_3 molecular symmetry) composed of uranyl tri-, di-, and monoperoxide polyhedra (Figure 6).

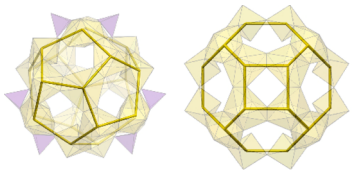

Figure 6. Polyhedral and graphical representation of $\{U_{20}P_6\}$ (left) and $\{U_{24}\}$ (right). Yellow and purple polyhedra represent uranium and phosphate, respectively. Yellow lines represent linkages between uranium polyhedra.

$\{U_{20}P_6\}$ is topologically closely related to the fullerene topology of $\{U_{20}\}$ that consists of 12 pentagons.[20] In contrast, the topology of $\{U_{24}\}$ is a sodalite-type cage consisting of six squares and eight hexagons (Figure 6). Furthermore, $\{U_{24}\}$ (idealized O_h molecular symmetry) is built from uranyl monoperoxide units $[(UO_2)(O_2)(OH)^-]$, such that each uranyl ion is coordinated by two peroxide moieties in a bidentate arrangement, as well as two hydroxyl groups. Stoichiometric transformation of six $\{U_{20}P_6\}$ to five $\{U_{24}\}$ would liberate six sulfate, 36 phosphate, and 42 peroxide groups. Given the very substantial topological rearrangement that is accomplished, we hypothesize that this reaction involves a complete breakdown of the original cluster into uranyl peroxide monomers and/or peroxide bridged uranyl dimers that condense via peroxide bound tetramers $[(UO_2)_4(O_2)_4]$, $\{U_4\}$ into $\{U_{24}\}$ (Figure 7). Recall that the NMR data do not reveal the presence of phosphate species other than $\{U_{20}P_6\}$ and free phosphate, which suggests that any long-lived intermediate fragments contain no phosphate. Given the lack of excess peroxide in the system, and because free peroxide is easily decomposed catalytically,[62,63] it is likely that peroxide is transferred among clusters as a ligand strongly complexed to the uranyl ion.

The time-resolved ^{31}P NMR experiments in conjunction with diffusion-ordered studies indicate release of phosphate in the early stages of the reaction (Figures 2 and 3). Furthermore, the noted increase of the phosphate signal intensity paired with its persistence indicates that liberated phosphate remains in solution through the course of the experiment rather than being incorporated into any of the observed solid phases. From a structural point of view, release of phosphate does not require a complete breakdown of the uranyl peroxide backbone of $\{U_{20}P_6\}$, but considering the topological differences (pentagons in $\{U_{20}P_6\}$ vs squares and hexagons in $\{U_{24}\}$) and the different number of uranyl ions in each cluster, a direct transformation of one into another is impossible. As such, we propose that the first step of the cluster-to-cluster transformation involves dissociation of the $\{U_{20}P_6\}$ into small uranyl peroxide units (Figure 7) accompanied by release of phosphate into solution.

The second and third steps of the proposed reaction scheme follow computationally predicted condensation trends where, in the presence of early alkali metal ions (Li, and Na), uranyl

DOI: 10.1021/acs.inorgchem.7b01095
Inorg. Chem. 2017, 56, 9602−9608

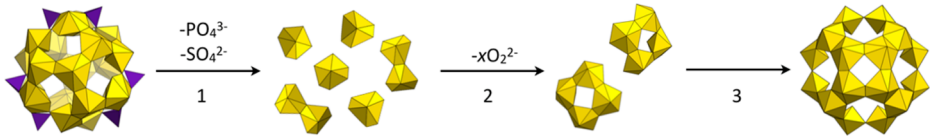

Figure 7. Proposed reaction mechanism for the spontaneous $\{U_{20}P_6\}$-to-$\{U_{24}\}$ transformation.

peroxide polyhedra are expected to form topological squares.[64,65] Keeping templating effects in mind while reviewing the topologies of previously reported uranyl peroxide nanoclusters,[17] one concludes that $\{U_{24}\}$ is the only feasible product. Moreover, the lack of evidence for formation of clusters containing both square and pentagonal motifs such as $\{U_{28a}\}$, $\{U_{30}\}$, or $\{U_{32}\}$ supports our hypothesis that $\{U_{20}P_6\}$ completely dissociates. Time-resolved Raman experiments suggest that the second and third steps of the proposed reaction occur in rapid succession due to the lack of signals corresponding to monomer or tetramer species in any of the collected spectra. Specifically, uranyl peroxide monomers have been a focus of a recent study showing that, upon coordination by three peroxide ligands, the signal corresponding to the symmetrical stretch of the uranyl undergoes a significant red shift to the 600−700 cm^{-1} region.[58] Interestingly, no free peroxide (875 cm^{-1}) is observed. The lack of such a signal is likely due to a combination of the low solubility of $\{U_{20}P_6\}$, the absence of added peroxide in the system, and the rapid decomposition of any liberated peroxide under basic conditions. Finally, SAXS results indicate retention of nanoscale objects in solution with calculated R_g values showing a trend of increasing molecular sizes consistent with $\{U_{20}P_6\}$-to-$\{U_{24}\}$ transformation (Figure 4). This result supports the hypothesis that the oligomeric species present upon dissociation of $\{U_{20}P_6\}$ rapidly condense to form $\{U_{24}\}$ and that peroxide is retained in the dissociation fragments and thus transferred among clusters.

The spontaneous cluster-to-cluster transformation described herein differs from previously reported examples. For instance, the transformation of the ε-Al_{13} Keggin polycation into Al_{30} occurs only in the presence of monomeric species.[44] Moreover, this transformation can be more accurately described as an isomerization reaction (ε-Al_{13} to δ-Al_{13}), followed by a monomer-promoted condensation of two δ-Al_{13} polycations, resulting in retention of the initial Keggin structure. Computational studies showed that, if uncatalyzed, direct isomerization among the Al_{13} Keggin isomers has an energy barrier of ca. 85 kJ/mol,[66] indicating that rotation of the triad can only be achieved via dissociation and reassembly, or via catalysis.[67] Consistent with this idea, the current work demonstrates a complete breakdown of the original cluster and a reassembly of uranyl peroxide polyhedra. Recently, a study of the dissolution of the uranyl peroxide mineral *studtite* noted that, under carefully controlled experimental conditions, a spontaneous transformation of $\{U_{28}\}$ to $\{U_{24}\}$ is detected. While this transformation appears similar to the one studied herein, it is important to note that the aforementioned transition was studied *in situ* and under cluster forming conditions. Notably, no experimental evidence was presented suggesting that dissolution of crystalline $\{U_{28}\}$ in water would lead to a similar transformation.

CONCLUSIONS

Herein, we utilized time-resolved SAXS, Raman, and ^{31}P NMR spectroscopy to follow an in situ cluster-to-cluster transformation of $\{U_{20}P_6\}$ to $\{U_{24}\}$. The unusual μ-η^1:η^2 bridging mode of the peroxide ligands present in the original cluster may contribute to its rapid decomposition ($t_{1/2}$ = 116.3 min) and reassembly into a nonfunctionalized uranyl peroxide cluster. It is evident that, upon decomposition of $\{U_{20}P_6\}$, most peroxide ligands are retained within the first coordination sphere of uranyl ions. Moreover, these simple oligomeric species show a strong tendency to spontaneously condense into highly charged, hollow, and symmetric clusters such as $\{U_{24}\}$. The reassembly/condensation steps of this reaction closely follow the computationally established trends based on cation templating effects. This study showcases the complexities of uranyl peroxide nanoclusters and highlights the need for further in-depth characterization of this family of macro-anions.

ASSOCIATED CONTENT

Supporting Information

The Supporting Information is available free of charge on the ACS Publications website at DOI: 10.1021/acs.inorgchem.7b01095.

Crystallographic data, Raman spectroscopy, magic-angle spinning NMR, diffusion-ordered spectroscopy, small-angle X-ray scattering, and references (PDF)

AUTHOR INFORMATION

Corresponding Author

*E-mail: pburns@nd.edu.

ORCID

Jie Qiu: 0000-0001-7131-4881
William H. Casey: 0000-0002-3275-6465
Peter C. Burns: 0000-0002-2319-9628

Author Contributions

M.D. and C.A.C. contributed equally.

Notes

The authors declare no competing financial interest.

ACKNOWLEDGMENTS

This material is based upon work supported as a part of the Materials Science of Actinides Center, and Energy Frontier Research Center funded by the U.S. Department of Energy, Office of Science, Office of Basic Energy Sciences, under Award No. DE-SC001089. Time-resolved ^{31}P NMR measurements were conducted at the Magnetic Resonance Research Center at the University of Notre Dame. ^{31}P DOSY NMR measurements were conducted at the Nuclear Magnetic Resonance Facility at UC Davis. MAS NMR measurements were conducted at the Keck NMR Facility at UC Davis. Raman spectroscopy measurements were conducted at the Materials Characterization Facility of the Center for Sustainable Energy at the University of Notre Dame.

DOI: 10.1021/acs.inorgchem.7b01095
Inorg. Chem. 2017, 56, 9602−9608

REFERENCES

(1) Pope, M. T. *Heteropoly and Isopoly Oxometalates*; Springer-Verlag: Berlin, 1983; p 180.
(2) Berzelius, J. J. Beitrag zur näheren Kenntniss des Molybdäns. *Ann. Phys. (Berlin, Ger.)* **1826**, *6*, 369−392.
(3) Keggin, J. F. Structure of the crystals of 12-phosphotungstic acid. *Nature* **1933**, *132*, 351−351.
(4) Keggin, J. F. The structure and formula of 12-phosphotungstic acid. *Proc. R. Soc. London, Ser. A* **1934**, *144*, 75−100.
(5) Bloor, L. G.; Solarska, R.; Bienkowski, K.; Kulesza, P. J.; Augustynski, J.; Symes, M. D.; Cronin, L. Solar-Driven Water Oxidation and Decoupled Hydrogen Production Mediated by an Electron-Coupled-Proton Buffer. *J. Am. Chem. Soc.* **2016**, *138*, 6707−6710.
(6) Lechner, M.; Guttel, R.; Streb, C. Challenges in polyoxometalate-mediated aerobic oxidation catalysis: catalyst development meets reactor design. *Dalton T.* **2016**, *45*, 16716−16726.
(7) Song, Y. F.; Tsunashima, R. Recent advances on polyoxometalate-based molecular and composite materials. *Chem. Soc. Rev.* **2012**, *41*, 7384−7402.
(8) She, S.; Bian, S. T.; Huo, R. C.; Chen, K.; Huang, Z. H.; Zhang, J. W.; Hao, J.; Wei, Y. G. Degradable Organically-Derivatized Polyoxometalate with Enhanced Activity against Glioblastoma Cell Line. *Sci. Rep.* **2016**, *6*, 33529.
(9) Luong, T. K. N.; Shestakova, P.; Absillis, G.; Parac-Vogt, T. N. Detailed Mechanism of Phosphoanhydride Bond Hydrolysis Promoted by a Binuclear Zr-IV-Substituted Keggin Polyoxometalate Elucidated by a Combination of ^{31}P, ^{31}P DOSY, and ^{31}P EXSY NMR Spectroscopy. *Inorg. Chem.* **2016**, *55*, 4864−4873.
(10) Nakhaei, A.; Davoodnia, A.; Morsali, A. Extraordinary catalytic activity of a Keplerate-type giant nanoporous isopolyoxomolybdate in the synthesis of 1,8-dioxo-octahydroxanthenes and 1,8-dioxodecahydroacridines. *Res. Chem. Intermed.* **2015**, *41*, 7815−7826.
(11) McGregor, D.; Burton-Pye, B. P.; Howell, R. C.; Mbomekalle, I. M.; Lukens, W. W.; Bian, F.; Mausolf, E.; Poineau, F.; Czerwinski, K. R.; Francesconi, L. C. Synthesis, Structure Elucidation, and Redox Properties of Tc-99 Complexes of Lacunary Wells-Dawson Polyoxometalates: Insights into Molecular Tc-99-Metal Oxide Interactions. *Inorg. Chem.* **2011**, *50*, 1670−1681.
(12) Long, D. L.; Burkholder, E.; Cronin, L. Polyoxometalate clusters, nanostructures and materials: From self assembly to designer materials and devices. *Chem. Soc. Rev.* **2007**, *36*, 105−121.
(13) Fang, X. K.; Hill, C. L. Multiple reversible protonation of polyoxoanion surfaces: Direct observation of dynamic structural effects from proton transfer. *Angew. Chem., Int. Ed.* **2007**, *46*, 3877−3880.
(14) Bunker, B. C.; Casey, W. H. *The Aqueous Chemistry of Oxides*, 1st ed.; Oxford University Press: New York, NY, 2016; p 12.
(15) Burns, P. C. Nanoscale uranium-based cage clusters inspired by uranium mineralogy. *Mineral. Mag.* **2011**, *75*, 1−25.
(16) Albrecht-Schmitt, T. E. Actinide materials adopt curvature: Nanotubules and nanospheres. *Angew. Chem., Int. Ed.* **2005**, *44*, 4836−4838.
(17) Qiu, J.; Burns, P. C. Clusters of Actinides with Oxide, Peroxide, or Hydroxide Bridges. *Chem. Rev.* **2013**, *113*, 1097−1120.
(18) Burns, P. C.; Kubatko, K. A.; Sigmon, G.; Fryer, B. J.; Gagnon, J. E.; Antonio, M. R.; Soderholm, L. Actinyl peroxide nanospheres. *Angew. Chem., Int. Ed.* **2005**, *44*, 2135−2139.
(19) Muller, A.; Gouzerh, P. Capsules with Highly Active Pores and Interiors: Versatile Platforms at the Nanoscale. *Chem. - Eur. J.* **2014**, *20*, 4862−4873.
(20) Sigmon, G. E.; Ling, J.; Unruh, D. K.; Moore-Shay, L.; Ward, M.; Weaver, B.; Burns, P. C. Uranyl-Peroxide Interactions Favor Nanocluster Self-Assembly. *J. Am. Chem. Soc.* **2009**, *131*, 16648−16649.
(21) Ling, J.; Qiu, J.; Szymanowski, J. E.; Burns, P. C. Low-symmetry uranyl pyrophosphate cage clusters. *Chem. - Eur. J.* **2011**, *17*, 2571−2574.
(22) Muller, A.; Krickemeyer, E.; Bogge, H.; Schmidtmann, M.; Peters, F. Organizational forms of matter: An inorganic super fullerene and keplerate based on molybdenum oxide. *Angew. Chem., Int. Ed.* **1998**, *37*, 3359−3363.
(23) Muller, A.; Sarkar, S.; Shah, S. Q.; Bogge, H.; Schmidtmann, M.; Kogerler, P.; Hauptfleisch, B.; Trautwein, A. X.; Schunemann, V. V.; Sarkar, S. Archimedean Synthesis and Magic Numbers: "Sizing" Giant Molybdenum-Oxide-Based Molecular Spheres of the Keplerate Type. *Angew. Chem., Int. Ed.* **1999**, *38*, 3238−3241.
(24) Ling, J.; Qiu, J.; Sigmon, G. E.; Ward, M.; Szymanowski, J. E.; Burns, P. C. Uranium pyrophosphate/methylenediphosphonate polyoxometalate cage clusters. *J. Am. Chem. Soc.* **2010**, *132*, 13395−133402.
(25) Ling, J.; Ozga, M.; Stoffer, M.; Burns, P. C. Uranyl peroxide pyrophosphate cage clusters with oxalate and nitrate bridges. *Dalton T.* **2012**, *41*, 7278−84.
(26) Muller, A.; Botar, B.; Bogge, H.; Kogerler, P.; Berkle, A. A potassium selective 'nanosponge' with well defined pores. *Chem. Commun.* **2002**, *24*, 2944−2945.
(27) Muller, A.; Krickemeyer, E.; Bogge, H.; Schmidtmann, M.; Roy, S.; Berkle, A. Changeable pore sizes allowing effective and specific recognition by a molybdenum-oxide based "Nanosponge": en route to sphere-surface and nanoporous-cluster chemistry. *Angew. Chem., Int. Ed.* **2002**, *41*, 3604−3609.
(28) Muller, A.; Das, S. K.; Talismanov, S.; Roy, S.; Beckmann, E.; Bogge, H.; Schmidtmann, M.; Merca, A.; Berkle, A.; Allouche, L.; Zhou, Y.; Zhang, L. Trapping cations in specific positions in tuneable "artificial cell" channels: new nanochemistry perspectives. *Angew. Chem., Int. Ed.* **2003**, *42*, 5039−5044.
(29) Gao, Y.; Szymanowski, J. E.; Sun, X.; Burns, P. C.; Liu, T. Thermal Responsive Ion Selectivity of Uranyl Peroxide Nanocages: An Inorganic Mimic of K^+ Ion Channels. *Angew. Chem., Int. Ed.* **2016**, *55*, 6887−6891.
(30) Wylie, E. M.; Peruski, K. M.; Weidman, J. L.; Phillip, W. A.; Burns, P. C. Ultrafiltration of Uranyl Peroxide Nanoclusters for the Separation of Uranium from Aqueous Solution. *ACS Appl. Mater. Interfaces* **2014**, *6*, 473−479.
(31) Wylie, E. M.; Peruski, K. M.; Prizio, S. E.; Bridges, A. N. A.; Rudisill, T. S.; Hobbs, D. T.; Phillip, W. A.; Burns, P. C. Processing used nuclear fuel with nanoscale control of uranium and ultrafiltration. *J. Nucl. Mater.* **2016**, *473*, 125−130.
(32) Burns, P. C.; Ewing, R. C.; Navrotsky, A. Nuclear Fuel in a Reactor Accident. *Science* **2012**, *335*, 1184−1188.
(33) Armstrong, C. R.; Nyman, M.; Shvareva, T.; Sigmon, G. E.; Burns, P. C.; Navrotsky, A. Uranyl peroxide enhanced nuclear fuel corrosion in seawater. *Proc. Natl. Acad. Sci. U. S. A.* **2012**, *109*, 1874−1877.
(34) Andersson, I.; Gorzsas, A.; Kerezsi, C.; Toth, I.; Pettersson, L. Speciation in the aqueous $H^+/H_2VO_4^-/H_2O_2$/phosphate system. *Dalton T* **2005**, *22*, 3658−3666.
(35) Hashimoto, M.; Andersson, I.; Pettersson, L. An equilibrium analysis of the aqueous H^+-MoO_4^{2-}-$(HP)O_3^{2-}$ and H^+-MoO_4^{2-}-$(HP)O_3^{2-}$-HPO_4^{2-} systems. *Dalton T* **2007**, *1*, 124−132.
(36) Hashimoto, M.; Andersson, I.; Pettersson, L. A ^{31}P NMR study of the H^+-MoO_4^{2-}-$(HP)O_3^{2-}$-HPO_4^{2-}-$(C_6H_5P)O_3^{2-}$-$(CH_3P)O_3^{2-}$ system at low Mo to P ratio - Formation of mixed-hetero X_2M_5-type polyanions. *Dalton T* **2009**, *17*, 3321−3327.
(37) Pettersson, L. Equilibria of Polyoxometalates in Aqueous Solution. In *Polyoxometalates: From Platonic Solids to Anti-Retroviral Activity*; Pope, M. T., Müller, A., Eds.; Springer: Dordrecht, Netherlands, 1994; pp 27−40.
(38) Chen, Z. Y.; Luan, Z. K.; Jia, Z. P.; Li, X. S. On the acid-base stability of Keggin Al_{13} and Al_{30} polymers in polyaluminum coagulants. *J. Mater. Sci.* **2009**, *44*, 3098−3111.
(39) Goberna-Ferron, S.; Soriano-Lopez, J.; Galan-Mascaros, J. R.; Nyman, M. Solution Speciation and Stability of Cobalt-Polyoxometalate Water Oxidation Catalysts by X-ray Scattering. *Eur. J. Inorg. Chem.* **2015**, *2015*, 2833−2840.
(40) Folkman, S. J.; Kirner, J. T.; Finke, R. G. Cobalt Polyoxometalate $Co_4V_2W_{18}O_{68}^{10-}$: A Critical Investigation of Its

DOI: 10.1021/acs.inorgchem.7b01095
Inorg. Chem. 2017, 56, 9602−9608

Synthesis, Purity, and Observed ^{51}V Quadrupolar NMR. *Inorg. Chem.* **2016**, *55*, 5343−5355.
(41) Lv, H. J.; Gao, Y. Z.; Guo, W. W.; Lauinger, S. M.; Chi, Y. N.; Bacsa, J.; Sullivan, K. P.; Wieliczko, M.; Musaev, D. G.; Hill, C. L. Cu-based Polyoxometalate Catalyst for Efficient Catalytic Hydrogen Evolution. *Inorg. Chem.* **2016**, *55*, 6750−6758.
(42) Cao, J.; Li, C. C.; Zhang, Z. X.; Xu, C.; Yan, J.; Cui, F. Y.; Hu, C. W. Intriguing Role of a Quaternary Ammonium Cation in the Dissociation Chemistry of Keggin Polyoxometalate Anions. *J. Am. Soc. Mass Spectrom.* **2012**, *23*, 366−374.
(43) Allouche, L.; Gerardin, C.; Loiseau, T.; Ferey, G.; Taulelle, F. Al-30: A giant aluminum polycation. *Angew. Chem., Int. Ed.* **2000**, *39*, 511−516.
(44) Allouche, L.; Taulelle, F. Conversion of Al-13 Keggin epsilon into Al-30: a reaction controlled by aluminum monomers. *Inorg. Chem. Commun.* **2003**, *6*, 1167−1170.
(45) Qiu, J.; Spano, T. L.; Dembowski, M.; Kokot, A. M.; Szymanowski, J. E. S.; Burns, P. C. Sulfate-Centered Sodium-Icosahedron-Templated Uranyl Peroxide Phosphate Cages with Uranyl Bridged by $\mu-\eta1:\eta2$ Peroxide. *Inorg. Chem.* **2017**, *56*, 1874−1880.
(46) Krause, L.; Herbst-Irmer, R.; Stalke, D. An empirical correction for the influence of low-energy contamination. *J. Appl. Crystallogr.* **2015**, *48*, 1907−1913.
(47) Sheldrick, G. M. SHELXT - Integrated space-group and crystal-structure determination. *Acta Crystallogr., Sect. A: Found. Adv.* **2015**, *71*, 3−8.
(48) Sheldrick, G. M. Crystal structure refinement with SHELXL. *Acta Crystallogr., Sect. C: Struct. Chem.* **2015**, *71*, 3−8.
(49) Nyman, M.; Alam, T. M. Dynamics of Uranyl Peroxide Nanocapsules. *J. Am. Chem. Soc.* **2012**, *134*, 20131−20138.
(50) Alam, T. M.; Liao, Z. L.; Zakharov, L. N.; Nyman, M. Solid-State Dynamics of Uranyl Polyoxometalates. *Chem. - Eur. J.* **2014**, *20*, 8302−8307.
(51) Alam, T. M.; Liao, Z. L.; Nyman, M.; Yates, J. Insight into Hydrogen Bonding of Uranyl Hydroxide Layers and Capsules by Use of H-1 Magic-Angle Spinning NMR Spectroscopy. *J. Phys. Chem. C* **2016**, *120*, 10675−10685.
(52) Oliveri, A. F.; Pilgrim, C. D.; Qiu, J.; Colla, C. A.; Burns, P. C.; Casey, W. H. Dynamic Phosphonic Bridges in Aqueous Uranyl Clusters. *Eur. J. Inorg. Chem.* **2016**, *2016*, 797−801.
(53) Luong, T. K.; Shestakova, P.; Absillis, G.; Parac-Vogt, T. N. Detailed Mechanism of Phosphoanhydride Bond Hydrolysis Promoted by a Binuclear Zr(IV)-Substituted Keggin Polyoxometalate Elucidated by a Combination of (31)P, (31)P DOSY, and (31)P EXSY NMR Spectroscopy. *Inorg. Chem.* **2016**, *55*, 4864−73.
(54) Izzet, G.; Abecassis, B.; Brouri, D.; Piot, M.; Matt, B.; Serapian, S. A.; Bo, C.; Proust, A. Hierarchical Self-Assembly of Polyoxometalate-Based Hybrids Driven by Metal Coordination and Electrostatic Interactions: From Discrete Supramolecular Species to Dense Monodisperse Nanoparticles. *J. Am. Chem. Soc.* **2016**, *138*, 5093−9.
(55) Johnson, R. L.; Ohlin, C. A.; Pellegrini, K.; Burns, P. C.; Casey, W. H. Dynamics of a Nanometer-Sized Uranyl Cluster in Solution. *Angew. Chem., Int. Ed.* **2013**, *52* (29), 7464−7467.
(56) Floquet, S.; Brun, S.; Lemonnier, J. F.; Henry, M.; Delsuc, M. A.; Prigent, Y.; Cadot, E.; Taulelle, F. Molecular Weights of Cyclic and Hollow Clusters Measured by DOSY NMR Spectroscopy. *J. Am. Chem. Soc.* **2009**, *131*, 17254−17259.
(57) Dembowski, M.; Colla, C. A.; Hickam, S.; Oliveri, A. F.; Szymanowski, J. E. S.; Oliver, A. G.; Casey, W. H.; Burns, P. C. Hierarchy of Pyrophosphate-Functionalized Uranyl Peroxide Nanocluster Synthesis. *Inorg. Chem.* **2017**, *56*, 5478−5487.
(58) Dembowski, M.; Bernales, V.; Qiu, J.; Hickam, S.; Gaspar, G.; Gagliardi, L.; Burns, P. C. Computationally-Guided Assignment of Unexpected Signals in the Raman Spectra of Uranyl Triperoxide Complexes. *Inorg. Chem.* **2017**, *56*, 1574−1580.
(59) McGrail, B. T.; Sigmon, G. E.; Jouffret, L. J.; Andrews, C. R.; Burns, P. C. Raman Spectroscopic and ESI-MS Characterization of Uranyl Peroxide Cage Clusters. *Inorg. Chem.* **2014**, *53*, 1562−1569.
(60) Falaise, C.; Nyman, M. The Key Role of U-28 in the Aqueous Self-Assembly of Uranyl Peroxide Nanocages. *Chem. - Eur. J.* **2016**, *22*, 14678−14687.
(61) Zanonato, P. L.; Di Bernardo, P.; Fischer, A.; Grenthe, I. Chemical equilibria in the UO_2^{2+}-H_2O_2-F^-/OH^- systems and possible solution precursors for the formation of $[Na_6(OH_2)_8]@[UO_2O_2)\text{-}F]_{24}^{18-}$ and $[Na_6(OH_2)_8]@[UO_2O_2OH]_{24}^{18-}$ clusters. *Dalton. T* **2013**, *42*, 10129−10137.
(62) Bruice, T. C.; Zipplies, M. F.; Lee, W. A. The Ph-Dependence of the Mechanism of Reaction of Hydrogen-Peroxide with a Non-aggregating, Non-Mu-Oxo Dimer-Forming Iron(Iii) Porphyrin in Water. *Proc. Natl. Acad. Sci. U. S. A.* **1986**, *83*, 4646−4649.
(63) Livingston, R. The rate of decomposition of hydrogen peroxide in concentrated solutions. *J. Phys. Chem.* **1943**, *47*, 260−264.
(64) Vlaisavljevich, B.; Gagliardi, L.; Burns, P. C. Understanding the Structure and Formation of Uranyl Peroxide Nanoclusters by Quantum Chemical Calculations. *J. Am. Chem. Soc.* **2010**, *132*, 14503−14508.
(65) Miro, P.; Pierrefixe, S.; Gicquel, M.; Gil, A.; Bo, C. On the Origin of the Cation Templated Self-Assembly of Uranyl-Peroxide Nanoclusters. *J. Am. Chem. Soc.* **2010**, *132*, 17787−17794.
(66) Andre Ohlin, C.; Rustad, J. R.; Casey, W. H. The energetics of isomerisation in Keggin-series aluminate cations. *Dalton Trans* **2014**, *43*, 14533−6.
(67) Smart, S. E.; Vaughn, J.; Pappas, I.; Pan, L. Controlled step-wise isomerization of the Keggin-type Al-13 and determination of the gamma-Al-13 structure. *Chem. Commun.* **2013**, *49*, 11352−11354.

DOI: 10.1021/acs.inorgchem.7b01095
Inorg. Chem. 2017, 56, 9602−9608